Linoleic acid: a natural feed compound against porcine epidemic diarrhea disease

Journal of Virology

Yang, Shanshan; Huang, Xin; Li, Shuxian; Wang, Caiying; Jansen, Christine A. et al

https://doi.org/10.1128/jvi.01700-23

AMERICAN SOCIETY FOR MICROBIOLOGY | Journal of Virology

Veterinary Microbiology | Full-Length Text

Linoleic acid: a natural feed compound against porcine epidemic diarrhea disease

Shanshan Yang,[1,2,3] Xin Huang,[1] Shuxian Li,[1,4] Caiying Wang,[1,2] Christine A. Jansen,[2] Huub F. J. Savelkoul,[2] Guangliang Liu[1,4]

AUTHOR AFFILIATIONS See affiliation list on p. 17.

ABSTRACT Porcine epidemic diarrhea virus (PEDV) is a pig coronavirus that causes severe diarrhea and high mortality in piglets, threatening the global pig industry. Clinically effective medicines against this virus are still not available. To find an optional natural feed compound, viral titers were detected, and the intestinal contents of specific pathogen-free pigs more effectively blocked PEDV invasion than those of the other two breeds investigated. Based on proteomic and metabolic analyses of the intestinal content, 10 metabolites were selected for further investigation, and linoleic acid (LA) was the most promising according to the selectivity index. By detecting viral gene expression, LA inhibited viral replication and release from Vero-E6 cells, mainly by influencing the PI3K pathway and, in particular, inhibiting AKT phosphorylation. In addition, LA bound to viral NSP5 and attenuated NSP5-activated AKT phosphorylation. In the *in vivo* pig experiment, oral administration of the higher dose of LA protected two-thirds of pigs from death, both of which completely recovered from the infection, while the lower dose of LA protected one-third of pigs from death but with the induction of severe diarrhea. In conclusion, LA can be used as a candidate medicine for the clinical prevention and treatment of PEDV, and its mechanism of inhibiting the PI3K signaling pathway provides some data support for the subsequent exploration of antiviral drugs for coronavirus infections.

IMPORTANCE Porcine epidemic diarrhea virus (PEDV) is a pig coronavirus that causes severe diarrhea and high mortality in piglets, but as no effective drugs are available, this virus threatens the pig industry. Here, we found that the intestinal contents of specific pathogen-free pigs effectively blocked PEDV invasion. Through proteomic and metabolic analyses of the intestinal contents, we screened 10 metabolites to investigate their function and found that linoleic acid (LA) significantly inhibited PEDV replication. Further investigations revealed that LA inhibited viral replication and release mainly by binding with PEDV NSP5 to regulate the PI3K pathway and, in particular, inhibiting AKT phosphorylation. *In vivo* experiments illustrated that orally administered LA protected pigs from PEDV challenge and severe diarrhea. These findings provide strong support for exploring antiviral drugs for coronavirus treatment.

KEYWORDS PEDV, coronavirus, antiviral drugs, linoleic acid, AKT

Porcine epidemic diarrhea virus (PEDV), a member of the alphacoronavirus family, is a virus that mainly infects the intestines of pigs and is the causative pathogen of PED. This disease is characterized by serious diarrhea, vomiting, dehydration, and even death in piglets less than 10 days old (1). PED is a major problem affecting the international pig industry that urgently needs to be resolved (2). To control PEDV infection, many antiviral medicines have been proposed. Quercetin 7-rhamnoside and tomatidine interfere with viral replication (3, 4), while griffithsin and phlorotannins prevent viral attachment of

Editor Tom Gallagher, Loyola University Chicago - Health Sciences Campus, Maywood, Illinois, USA

Address correspondence to Guangliang Liu, LiuGuangliang01@caas.cn.

The authors declare no conflict of interest.

See the funding table on p. 17.

Received 30 October 2023
Accepted 31 October 2023
Published 27 November 2023

PEDV to Vero cells (5, 6). To date, none of these drugs have been applied for the clinical treatment of PEDV infection.

The intestinal microenvironment, colonized by the microbiota, plays a crucial role in providing immunity and defending against pathogens (7, 8). The gut microbiota and its metabolites have been reported to influence viral infections (9), impacting viral genetic recombination, host cell proliferation, and the immunoregulatory microenvironment (10). Therefore, we speculate that antiviral components may be present in the intestinal microenvironment. Until now, only the intestinal component surfactin has shown significant effects against PEDV infection by reducing the membrane fusion rate (11).

In this study, we searched for potentially new medicines that target the intestinal microenvironment, where PEDV mainly invades. As a result, the metabolite linoleic acid (LA) was screened out from the intestinal content as an antiviral natural compound to inhibit PEDV infection. Furthermore, the antiviral mechanism of LA was mainly focused on inhibiting the PI3K/AKT/mTOR pathway. This pathway regulates signal transduction and numerous biological processes, such as apoptosis, cell proliferation, and metabolism (12). This research not only offers a novel methodology for managing PEDV infection but also furnishes additional insights into preventing coronavirus infection.

RESULTS

Intestinal content blocks PEDV infection

The Cell Counting Kit-8 (CCK-8) assay was first utilized to confirm that the filtered intestinal contents had no toxic effect on Vero-E6 cells for 24 h (Fig. S1). To identify whether the intestinal content could inhibit viral infection, its effect on Vero cell infection with PEDV, herpes simplex virus (HSV), vesicular stomatitis virus (VSV), and Sendai virus (SeV) was assessed. Compared to the mock-infected group, different viral infections were reduced in Vero-E6 cells by a factor of tens to hundreds of times, as determined by the median tissue culture infectious dose ($TCID_{50}$) and attenuated cytopathic effect analyses (Fig. 1A through D). The antiviral effects of the intestinal contents of three pig breeds [TC, specific pathogen-free pig (SPF), and *Sus scrofa* (SS)] were compared to determine which ingredient had the strongest effect on PEDV. Results showed that the intestinal contents of SPF pigs had the strongest antiviral effect, as evidenced by the lowest viral titer (from $10^{5.606}$ to $10^{0.4012}$) (Fig. 1E) and fewest viral copies (from $10^{7.21}$ to $10^{1.714}$) (Fig. 1F). Additionally, fluorescence staining of the N protein of PEDV showed that incubation with the intestinal content of SPF pigs significantly reduced the presence of the virus compared to the mock-infected group (Fig. 1G).

Acids are responsible for suppressing viral infections

To identify the components of the intestinal content that are effective in inhibiting virus infection, proteomic and metabolic analyses were conducted on the three species of pigs. Analysis revealed that 1,032 proteins were shared among the three species, which were found to be enriched in the ribosome, amino acid synthesis, and carbon metabolism pathways (Fig. 2A; Fig. S2A). Gene Ontology (GO) annotations showed that these shared proteins were involved in carbohydrate catabolic processes and the cellular response to oxygen-containing compounds (Fig. S2B). Results from the local string network cluster suggested that these proteins were all related to carbon metabolism and acid formation (Fig. 2B). After removing unidentified substances, a total of 96 metabolites were found to be shared among the intestinal metabolites from the three pig breeds (Fig. 2C). Most of these metabolites are involved in the citrate cycle, while the Warburg effect and biosynthesis of unsaturated fatty acids were listed closely thereafter (Fig. 2D).

To further refine the putative metabolites with antiviral activities, a heatmap was created with the top 30 shared metabolites (Fig. 2E). Myo-inositol was the most abundant, while lactic acid, succinic acid, glutamic acid, linoleic acid, and palmitic acid were involved in the acid metabolism pathways. Furthermore, stigmasterol, cholic acid, elaidic acid, and β-sitosterol were more abundant in the SPF group than in the TC group, which

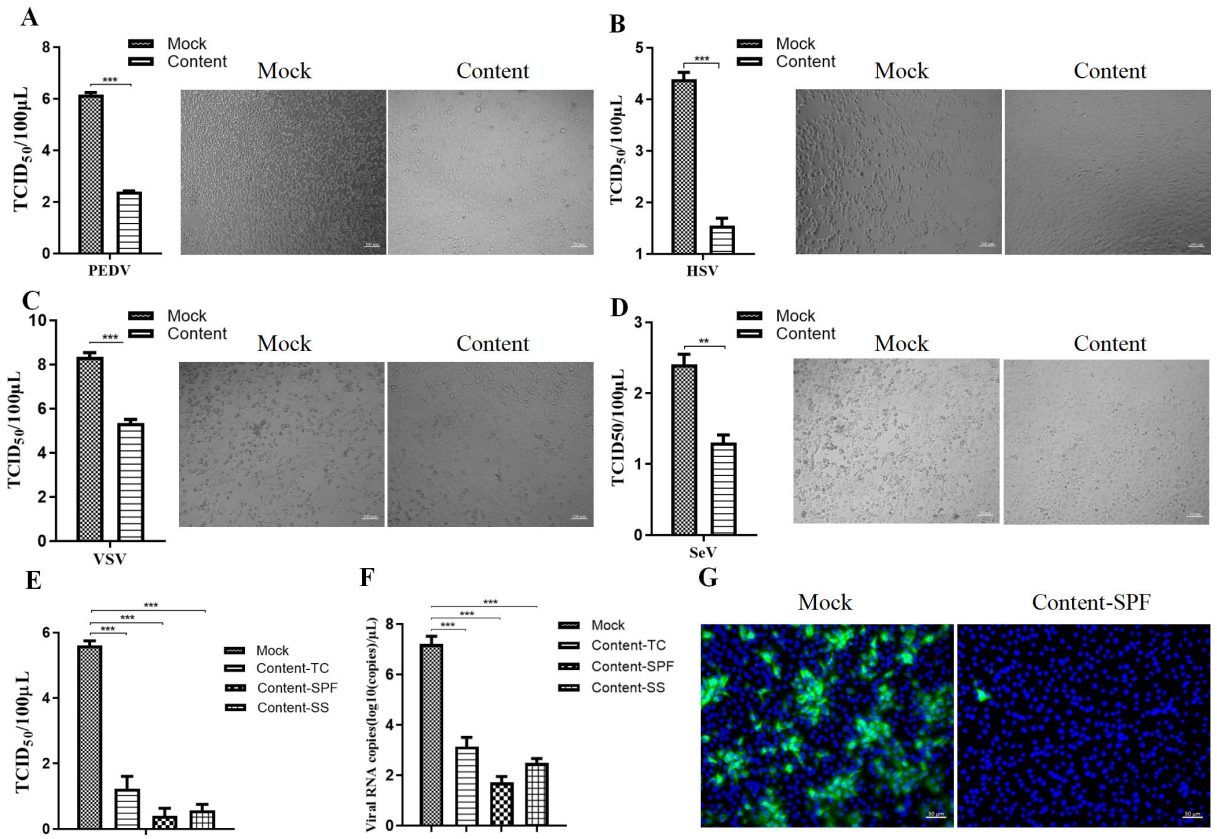

FIG 1 Intestinal content blocks PEDV infection. (A–D) Different viruses (PEDV, HSV, VSV, and SeV) mixed with intestinal content or phosphate buffer saline (PBS) as a mock control were separately incubated with Vero-E6 cells for 24 h. The cell supernatants were collected and evaluated by the $TCID_{50}$ assay. The cellular condition was recorded. (E) PEDV mixed with intestinal contents from different species of pigs (TC, SPF, SS) was separately incubated with Vero-E6 cells for 24 h. The cell supernatants were collected and evaluated by the $TCID_{50}$ assay. (F) Cells were collected for RNA extraction and real-time quantitative PCR detection. (G) PEDV mixed with the intestinal content of SPF pigs was incubated with Vero-E6 cells for 24 h. The viruses in the cells were examined by immunofluorescence assay (IFA). *P* value less than 0.001 is designated with three asterisks (***). *P* value less than 0.01 is designated with two asterisks (**).

had the weakest antiviral effect. Hence, these 10 metabolites were selected for further analysis.

Linoleic acid inhibits PEDV replication and release

The CCK-8 assay was used to evaluate the toxic effect of these 10 metabolites on Vero-E6 cells. The concentration of each metabolite that caused 50% cell death (CC_{50}) and 50% effective concentration (EC_{50}) was determined (Fig. S3A). Real-time quantitative PCR (RT-qPCR) results showed that stigmasterol, succinic acid, and linoleic acid treatments resulted in decreased virus levels compared to the mock-infected group (Fig. 3A). Succinic acid and linoleic acid inhibited viruses in a dose-dependent manner, while stigmasterol blocked viral infection at a specific concentration (Fig. 3B). The selectivity index (SI), calculated as the ratio of CC_{50} to EC_{50}, indicated that LA had the strongest inhibitory effect on viral replication (Fig. 3C; Fig. S3A).

To confirm the inhibitory effect of LA, a dose-dependent fluorescence reduction was observed in LA-treated cells using immunofluorescence assay (IFA) (Fig. 3D). Furthermore, $TCID_{50}$ analysis, viral copy detection, and western blotting of Vero-E6 cells infected with PEDV demonstrated that LA effectively inhibited PEDV infection (Fig. 3E, F and G). Additionally, RT-qPCR and western blotting showed that LA was able to inhibit PEDV infection in IPEC-J2 (Fig. S3B and Fig. S3C). Moreover, continuous treatment with LA effectively decreased the $TCID_{50}$ values of the released virus (Fig. 3H) and reduced the green fluorescent signals in the IFA results (Fig. 3I). By following the steps outlined in Fig.

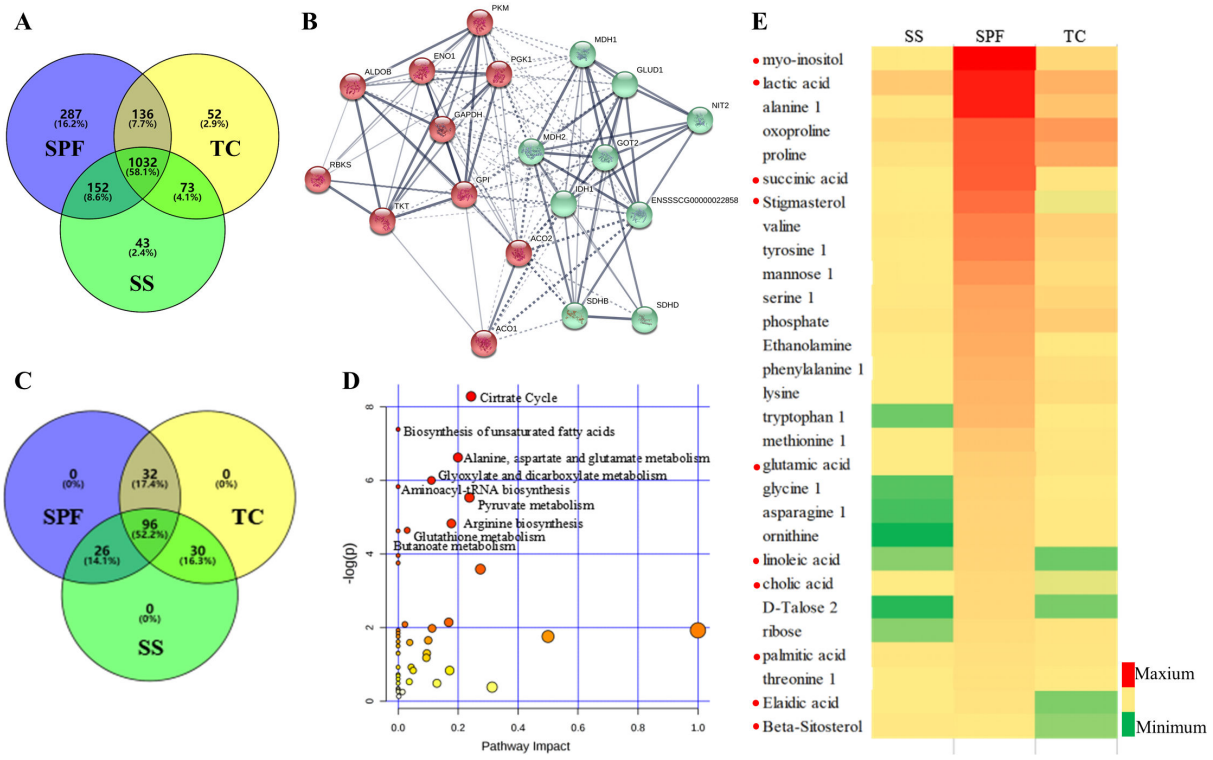

FIG 2 Acids are responsible for suppressing viral infections. (A) A Venn diagram of the proteins in the intestinal contents of three pig breeds is shown. (B) The local string network cluster was created by Cytoscape. The red proteins are carbohydrate metabolism-related enzymes, and the green proteins are dehydrogenases, suggesting the formation of many acid substances. (C) A Venn diagram of the metabolites in the intestinal contents of three pig breeds is shown. (D) Pathway analysis of mutual metabolites among three species of pigs was performed in MetaboAnalyst. The metabolome view on the left shows all matched pathways according to the *P* values from the pathway enrichment analysis and pathway impact values from the pathway topology analysis. Colors (varying from yellow to red) indicate different levels of significance (red denotes a more significant difference). (E) The top 30 mutual metabolites are listed and shown as a heatmap. The color changes from green to yellow to red, indicating an increasing proportion of metabolites.

3J, RT-qPCR results (Fig. 3K) showed that pretreatment with LA significantly inhibited viral replication. LA inhibited PEDV replication and viral release while not impacting attachment or internalization.

Linoleic acid inhibits PEDV infection via the PI3K/AKT/mTOR[Ed1] pathway

Swiss Target Prediction was utilized to assess the impact of LA on host proteins (13). These proteins were mostly concentrated in the fatty acid-binding protein family, followed by nuclear receptors and enzymes (Fig. 4A). Notable proteins included PPARγ, FABP4, FFAR1, LAMP1, and SREBP1c. LA treatment was found to reduce the mRNA expression levels of FABP4, LAMP1, PPARγ, and SREBP1c when inhibiting PEDV infection (Fig. 4B). Remarkably, LA treatment alone caused a decrease in the expression levels of LAMP1, PPARγ, and SREBP1c, even without PEDV (Fig. 4C). Furthermore, PEDV infection alone was seen to partly downregulate the expression of LAMP1 and SREBP1c (Fig. 4D). Our findings suggest that LA may inhibit viral infection by suppressing the expression of LAMP1, PPARγ, and SREBP1c. Fig. S4A through S4E demonstrate that overexpression of LAMP1, PPARγ, and SREBP1c diminishes LA's capability to impede PEDV replication, as evidenced by the decrease in both mRNA and protein levels.

Our results demonstrated the antiviral properties of chloroquine (CQ) as an inhibitor of LAMP1 by showing that CQ treatment caused a decrease in expression of the M gene (Fig. S4B), a reduction in N protein expression (Fig. S4C), and a decline in viral titers (Fig. S4D). Overexpression of LAMP1, PPARγ, and SREBP1c could activate the PI3K/AKT/mTOR pathway (Fig. 4F), which is known to be involved in cell metabolism and proliferation, with PPARγ and SREBP1c being particularly essential (12). This activation was mainly

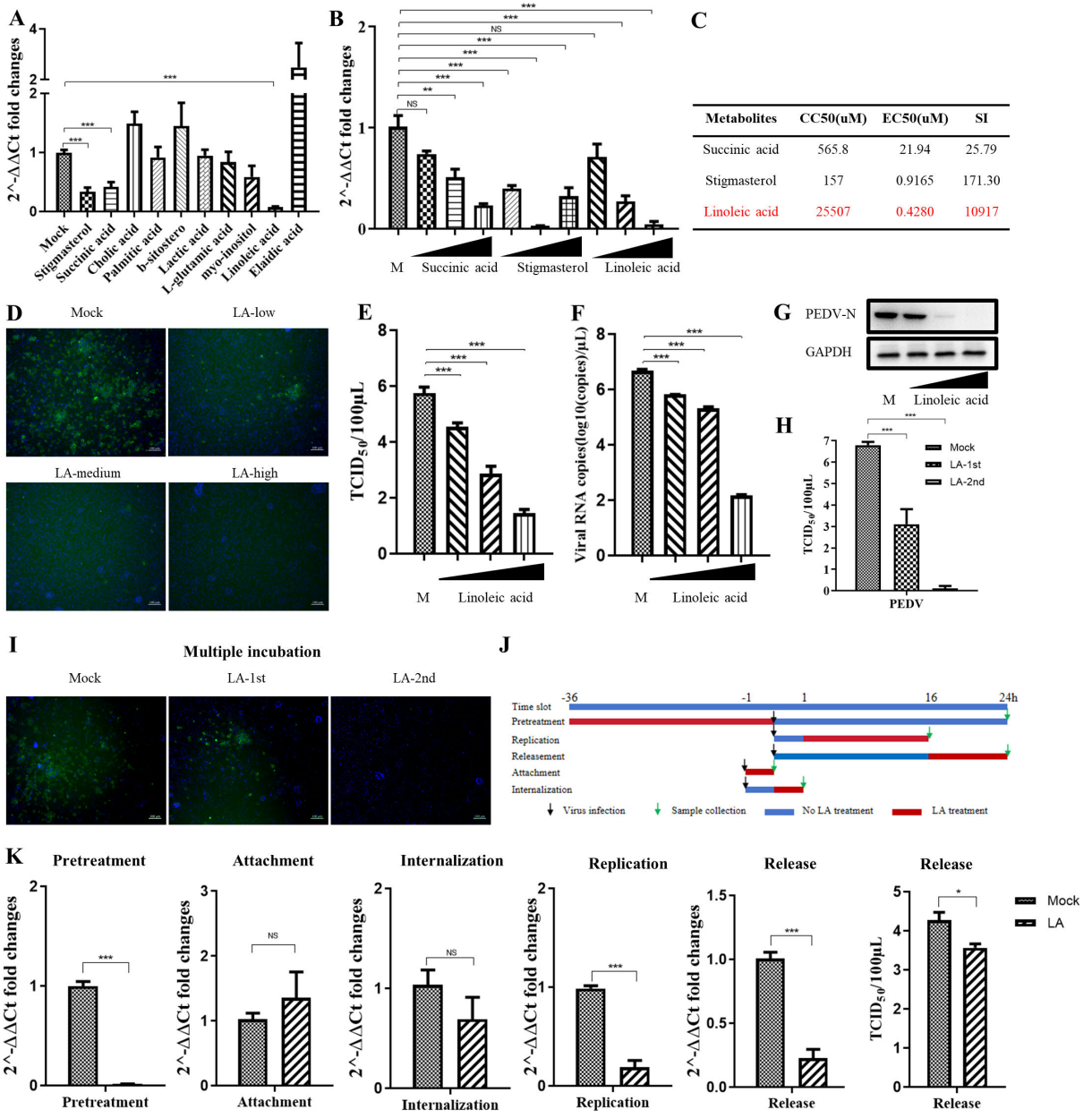

FIG 3 Linoleic acid inhibits PEDV replication and release. (A) RT-qPCR was utilized to detect viral M gene expression in cells that were incubated with PEDV and mixed with different metabolites at the highest concentration that showed no toxicity on cells for 24 h. (B) RT-qPCR was utilized to detect viral gene expression in cells that were incubated with PEDV mixed with different doses of metabolites. Succinic acid: 0.25, 2.5, 0.25 mM; stigmasterol: 1, 3, 6 μM; and linoleic acid: 0.1, 1, 6 μM. (C) Statistical analysis of the CC_{50} and EC_{50} data in Fig. S2A. SI, ratio of CC_{50} to EC_{50}. (D–G) IFA, $TCID_{50}$, viral copies, and western blotting results from PEDV-infected Vero-E6 cells treated with different doses of LA (1, 6, 10 μM) in comparison to phosphate buffer saline (PBS) as a control. (H and I) $TCID_{50}$ and IFA results showed the antiviral effect after continuous treatment with LA. (J) Detailed representation of the LA treatment schedule at different points during the infection cycle and when cell samples were collected for further analysis. For pretreatment, the treatment was added for 36 h and then washed away before viral incubation for 24 h. For replication, treatment was added after viral infection for 1 h and stopped at 16 h. For release, treatment was added after viral infection for 16 h and stopped at 24 h. For attachment, treatment mixed with virus was incubated at 4°C for 1 h. For internalization, treatment was added 1 h after viral infection at 4°C for 1 h. According to the above method, the cells were washed and collected for RT-qPCR analysis. (K) According to the above method, the cells were washed and collected for RT-qPCR analysis, and the supernatants were collected for RT-qPCR analysis and $TCID_{50}$ determination. *P* value less than 0.001 is designated with three asterisks (***). *P* value less than 0.01 is designated with two asterisks (**). *P* value less than 0.05 is designated with one asterisk (*).

observed at the protein level, with little effect on the mRNA levels of PI3K, AKT, and mTOR (Fig. S4E). Furthermore, LA treatment inhibited the mRNA and protein expression

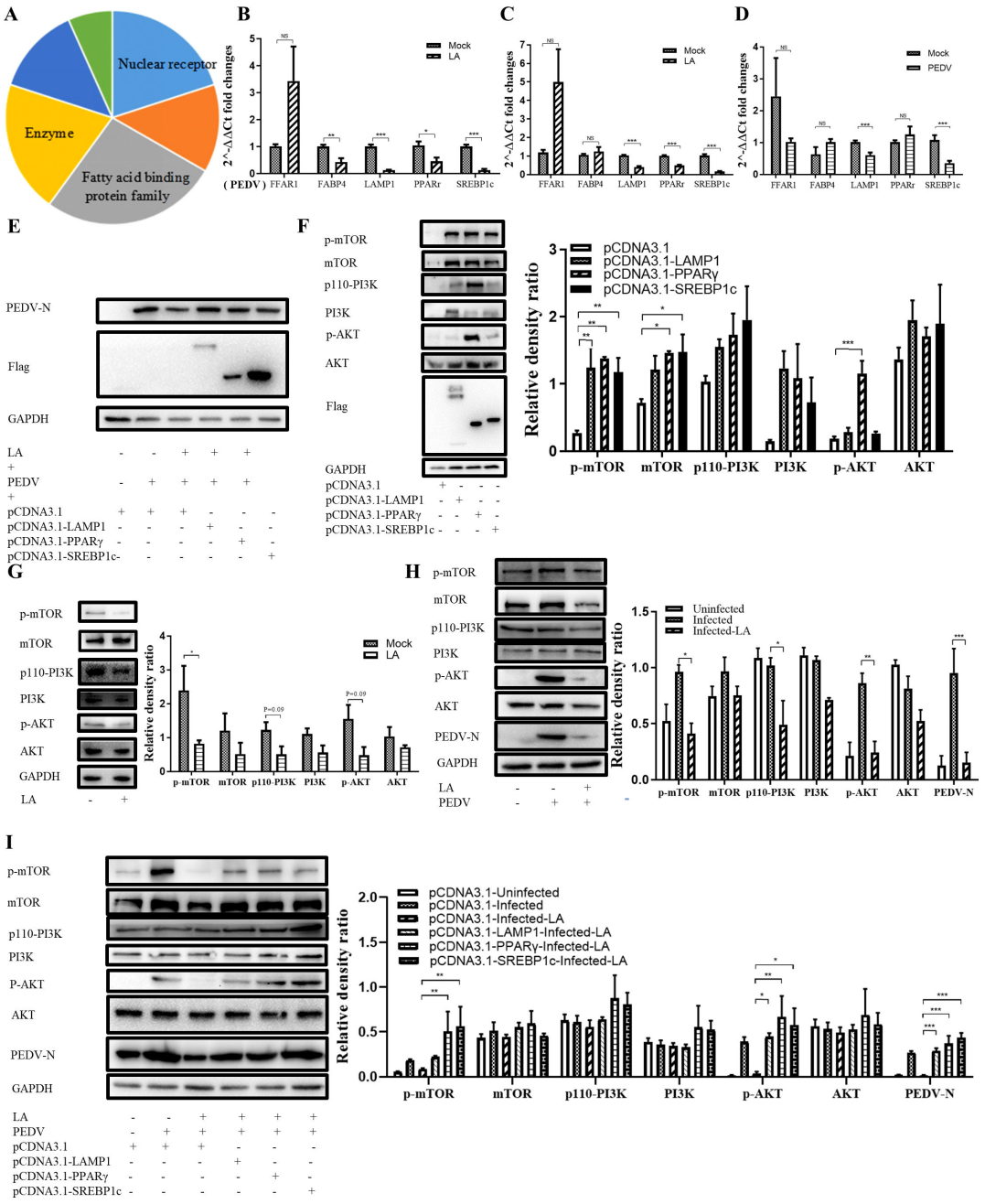

FIG 4 Linoleic acid inhibits PEDV infection via the PI3K/AKT/mTOR pathway. (A) The pie chart data were derived from the LA-related proteins analyzed by the Swiss Target Prediction tool. (B, C and D) RT-qPCR was utilized to detect viral gene expression levels in cells treated with PEDV mixed with LA, LA alone, or PEDV alone. (E) Viral protein expression levels were detected after transfection of LAMP1, PPARγ, and SREBP1c plasmids prior to viral infection by western blotting. (F) PI3K pathway protein expression levels were detected after transfection of the LAMP1, PPARγ, and SREBP1c by western blotting. The abbreviations p-AKT and p-mTOR indicate the phosphorylation status of AKT and mTOR, respectively. p110-PI3K is the catalytic subunit (p110 protein) of PI3K. Grayscale analysis of triplicate results is shown aside from the bands. (G) Western blotting was applied to examine how LA can influence key molecules in the PI3K pathway and the levels of the related proteins. (H) Western blotting was applied to examine how key PI3K pathway protein levels were influenced when the virus was inhibited by LA. Compared to infected groups, LA's inhibitory ability was shown as star marks. (I) PI3K pathway protein expression levels were detected by western blotting when the virus was restored after transfection of the LAMP1, PPARγ, and SREBP1c plasmids. *P* value less than 0.001 is designated with three asterisks (***). *P* value less than 0.01 is designated with two asterisks (**). *P* value less than 0.05 is designated with one asterisk (*).

levels of the PI3K/AKT/mTOR pathway (Fig. 4G; Fig. S4F). Following LA's inhibition of viral infection, the PI3K/AKT/mTOR signaling pathway was also suppressed at both the protein and mRNA levels (Fig. 4H; Fig. S4G). Overexpression of LAMP1, PPARγ, and SREBP1c

reversed the inhibitory effect of LA on viral infection, with the PI3K/AKT/mTOR signaling pathway being activated (Fig. 4I). Hence, we suspected that the inhibitory activity of LA may depend on the impairment of the PI3K/AKT/mTOR signaling pathway.

Inhibition of the PI3K/AKT/mTOR pathway suppresses viral infection

To further test this hypothesis, selective inhibitors of LAMP1, PPARγ, SREBP1c, PI3K, AKT, and mTOR were applied before viral infection, and the results of RT-qPCR (Fig. 5A), $TCID_{50}$ (Fig. 5B), and western blotting analyses (Fig. 5C) suggested that the inhibition of the pathway could effectively restrain viral infection. Moreover, LA and these inhibitors were seen to impede CV777 PEDV infection in Vero-E6 cells, as evidenced by decreased PEDV-N protein expression and viral titers, as well as diminished fluorescence (Fig. 5D, E and F; Fig. S5A). LA treatment and these inhibitors also inhibited PEDV-N protein expression levels in infected IPEC-J2 cells (Fig. S5B and Fig. S5C). These data collectively demonstrated that inhibition of the PI3K/AKT/mTOR pathway suppressed PEDV infection.

The antiviral effect of linoleic acid mainly depends on AKT phosphorylation

To further study how LA inhibits PEDV by influencing the PI3K/AKT/mTOR signaling pathway, the expression levels of PI3K, AKT, and mTOR after PEDV infection were determined. The protein levels of the phosphorylated active forms of mTOR and AKT increased (Fig. 6A), and the mRNA levels of AKT decreased (Fig. S6A). Additionally, the mTOR activator could restore the viral infection that had been inhibited by LA at both the mRNA level (Fig. S6B) and protein level (Fig. 6B). Overexpression of AKT also weakened the inhibitory effect of LA on viral infection, as shown in Fig. S6C and Fig. 6C. Subsequent analysis revealed that UV-inactivated PEDV did not induce AKT phosphorylation and only partly inhibited mTOR phosphorylation (Fig. 6D; Fig. S6D and Fig. S6E). This suggested that the inhibition of AKT phosphorylation was a major factor in the antiviral effect of LA. To further confirm that phosphorylation of AKT is essential for viral infection, the amino acid at the key phosphorylation site (Ser473) of AKT was mutated (14) (Fig. S6F). RT-qPCR and western blotting results both indicated that the mutant AKT was unable to reverse the inhibitory effect of LA (Fig. 6E; Fig. S6G). Moreover, transfection of AKT siRNA inhibited AKT phosphorylation and viral infection (Fig. 6F).

To investigate the LA-mediated phosphorylation of AKT in viral infection, inhibitors such as carbobenzoxy-valyl-alanyl-aspartyl-[O-methyl]-fluoromethylketone (Z-VAD-FMK), 3-methyladenine (3-MA), and MG132 were employed to observe the pathway by which phosphorylated proteins were degraded. The western blotting results revealed that the addition of Z-VAD-FMK partially recovered LA-impeded infection, independent of apoptosis (Fig. S6H and I). Except for the hypothesis, nonstructural proteins may activate AKT phosphorylation, as live viruses could activate AKT phosphorylation, whereas inactivated viruses could not. A molecular docking simulation conducted with LA showed that all structural and nonstructural viral proteins were involved, and proteins exhibiting a binding energy of over 3 kcal/mol were further analyzed. It was found that S2, M, NSP1, and NSP5 could directly interact with LA (Fig. 6G through J). As the expression of NSP5 *in vitro* was greater than that of NSP1, NSP5 was selected for further study. Dynamic analysis indicated that LA could combine with NSP5 via amino acids 294 or 290. Additionally, the results of isothermal titration calorimetry (ITC) showed that eukaryotically expressed NSP5 could interact with LA (Fig. 6H). Subsequently, western blotting results showed that NSP5 successfully activated AKT phosphorylation (Fig. 6I). This activation was effectively inhibited after LA treatment (Fig. 6J). To understand how LA inhibited NSP5-induced AKT phosphorylation, NSP5 was further found to interact with AKT via confocal microscopy and coimmunoprecipitation methods (Fig. 6K and L). Molecular docking results further revealed that amino acids at sites 290 and 294 are situated in the pocket between NSP5 and AKT. Therefore, these data suggest that LA inhibits NSP5-induced AKT phosphorylation by interacting with NSP5.

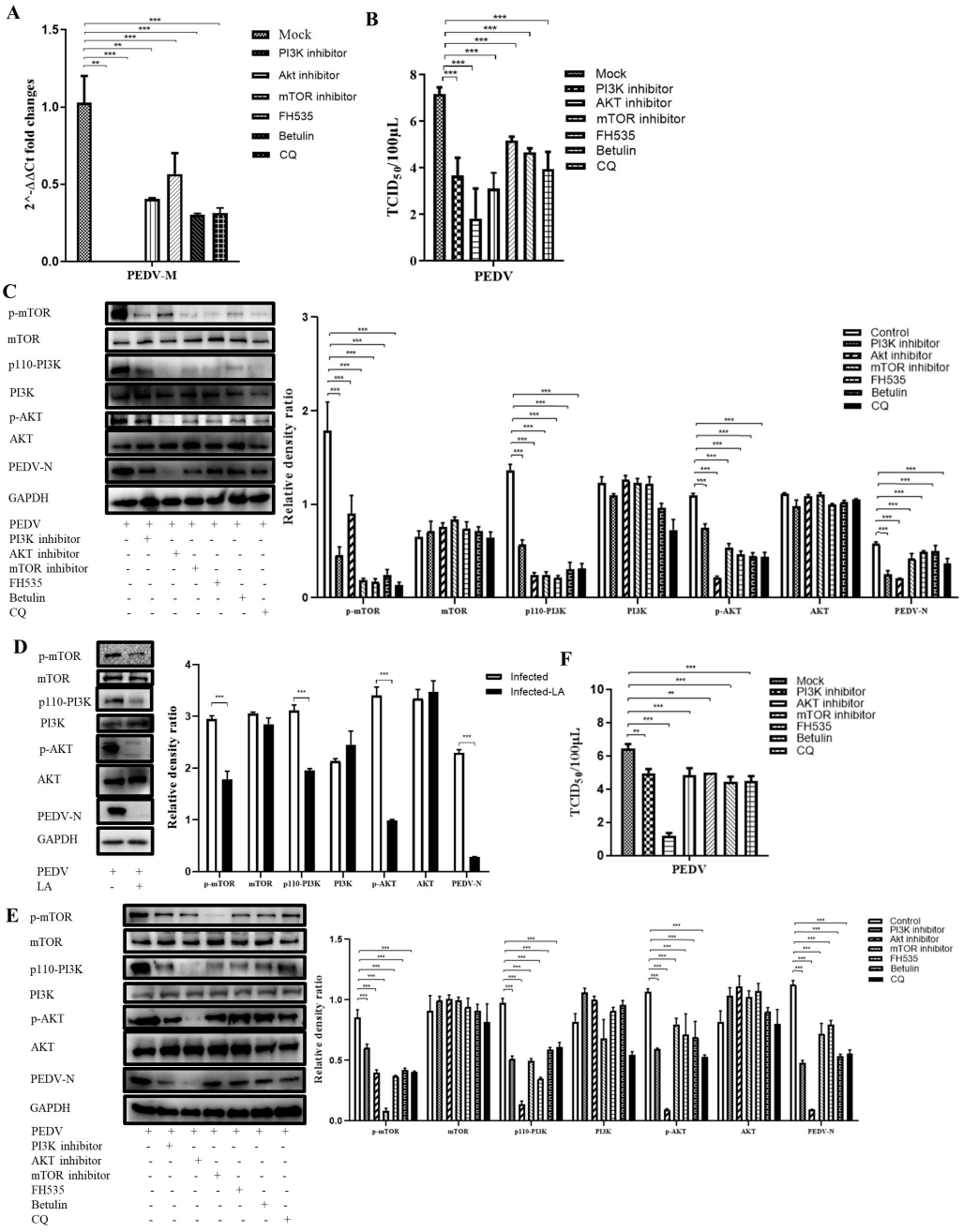

FIG 5 Inhibition of the PI3K/AKT/mTOR pathway suppresses viral infection. (A through C) RT-qPCR, $TCID_{50}$, and western blotting were utilized to detect viral infection after treatment with various inhibitors. PI3K inhibitor concentration: 0.33 μM. AKT inhibitor concentration: 10 μM. mTOR inhibitor concentration: 3 μM. FH535 (an inhibitor of PPARγ) concentration: 5 μM; betulin (an inhibitor of SREBP1c) concentration: 1 μM; CQ (an inhibitor of LAMP1) concentration: 2 μM. Grayscale analysis from triplicate results is shown aside from the bands. (D through F) $TCID_{50}$ and western blotting were utilized to detect viral infection (PEDV strain CV777) after treatment with LA and various inhibitors. *P* value less than 0.001 is designated with three asterisks (***). *P* value less than 0.01 is designated with two asterisks (**). *P* value less than 0.05 is designated with one asterisk (*).

Linoleic acid exhibits antiviral effects against PEDV infection in animal models

To explore whether LA has antiviral activity *in vivo*, a pig experiment was performed (Fig. 7A). The survival curve showed that the addition of a low dose of LA protected one

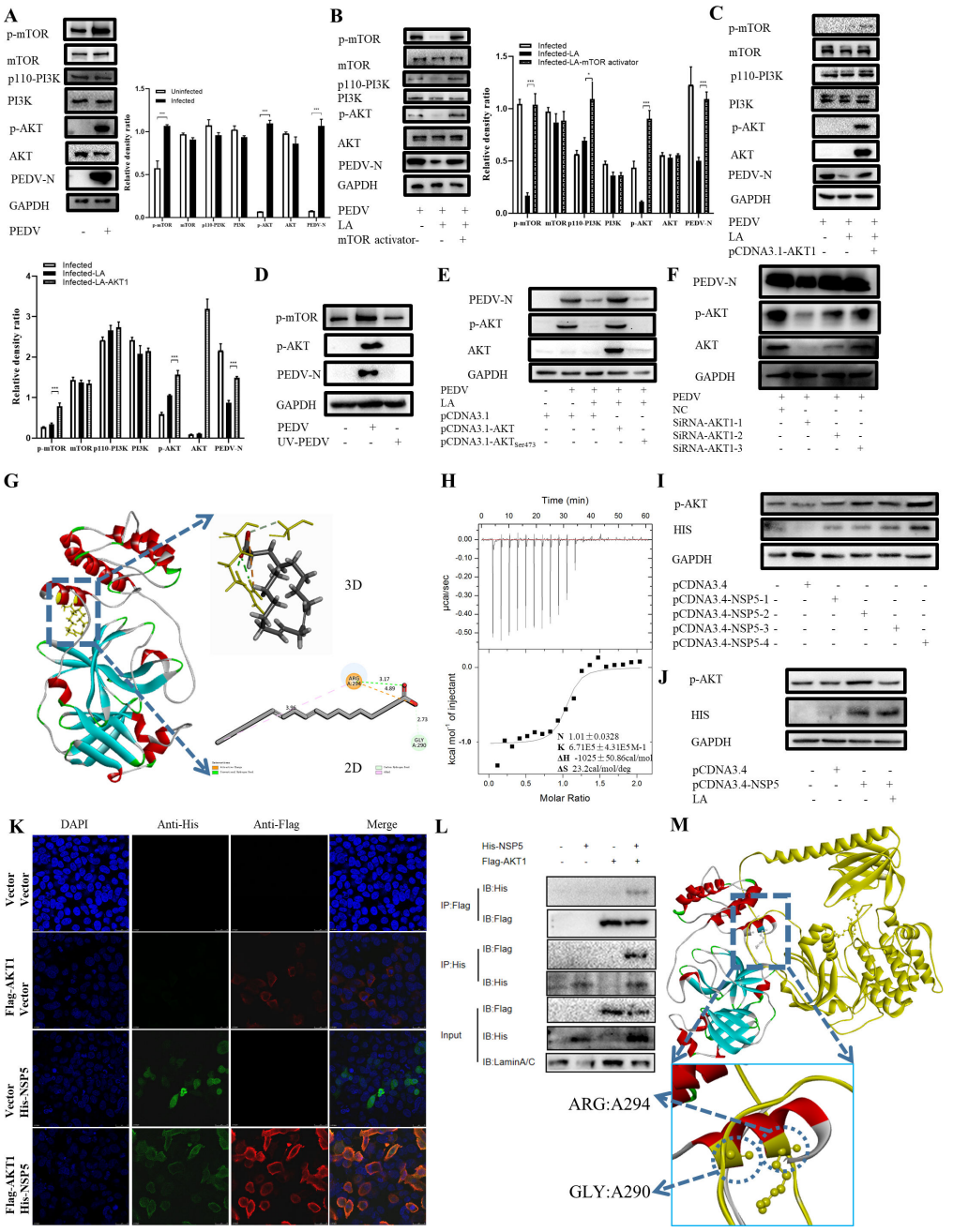

FIG 6 The antiviral effect of linoleic acid mainly depends on AKT phosphorylation. (A) Western blotting was applied to examine how PEDV infection could influence the expression levels of key PI3K pathway proteins. (B) Western blotting was applied to examine how the LA-reduced viral infection could be restored by an mTOR activator. The mTOR activator concentration was 3 μM. (C) Western blotting was applied to examine how the LA-reduced viral infection was restored by AKT overexpression. (D) Western blotting was applied to examine the viral protein and phosphorylated AKT expression levels after an inactivated viral infection in comparison to a control viral infection. (E) Western blotting was applied to examine whether AKT_{Ser473} overexpression restored LA-inhibited viral infection. (F) Western blotting was applied to examine whether AKT siRNA overexpression inhibited viral infection. (G) The combined results of LA and viral proteins were analyzed by AutoDock Vina and visualized by PyMOL and Discovery Studio. LA is shown in yellow. (H) The direct interaction between LA and NSP5 was analyzed and characterized by isothermal titration calorimetry. The value on the Y-axis is the energy released after their combination. (I) Phosphorylated AKT expression levels were detected by western blotting after transfection with NSP5 plasmids. (J) Phosphorylated AKT expression levels were detected by western blotting after transfection with NSP5 plasmids and LA treatment. (K and L) The interaction between NSP5 and AKT1 was identified by confocal microscopy and

(Continued on next page)

FIG 6 (Continued)

immunoprecipitation. (M) The combined results of AKT1 and NSP5 were analyzed by GRAMM docking and visualized by Discovery Studio. *P* value less than 0.001 is designated with three asterisks (***). *P* value less than 0.01 is designated with two asterisks (**). *P* value less than 0.05 is designated with one asterisk (*).

pig from death, while a high dose of LA led to the successful recovery of two pigs (Fig. 7B), which was accompanied by no viral shedding (Fig. 7D) and no diarrheal symptoms determined by the restored wet and dry ratio (Fig. 7C), low fecal consistency scores (Fig. S7A), and an increase in weight (Fig. S7B) in recovered pigs. Additionally, no viral load was observed in the intestines of piglets treated with a high dose of LA, as shown in Fig. 7E.

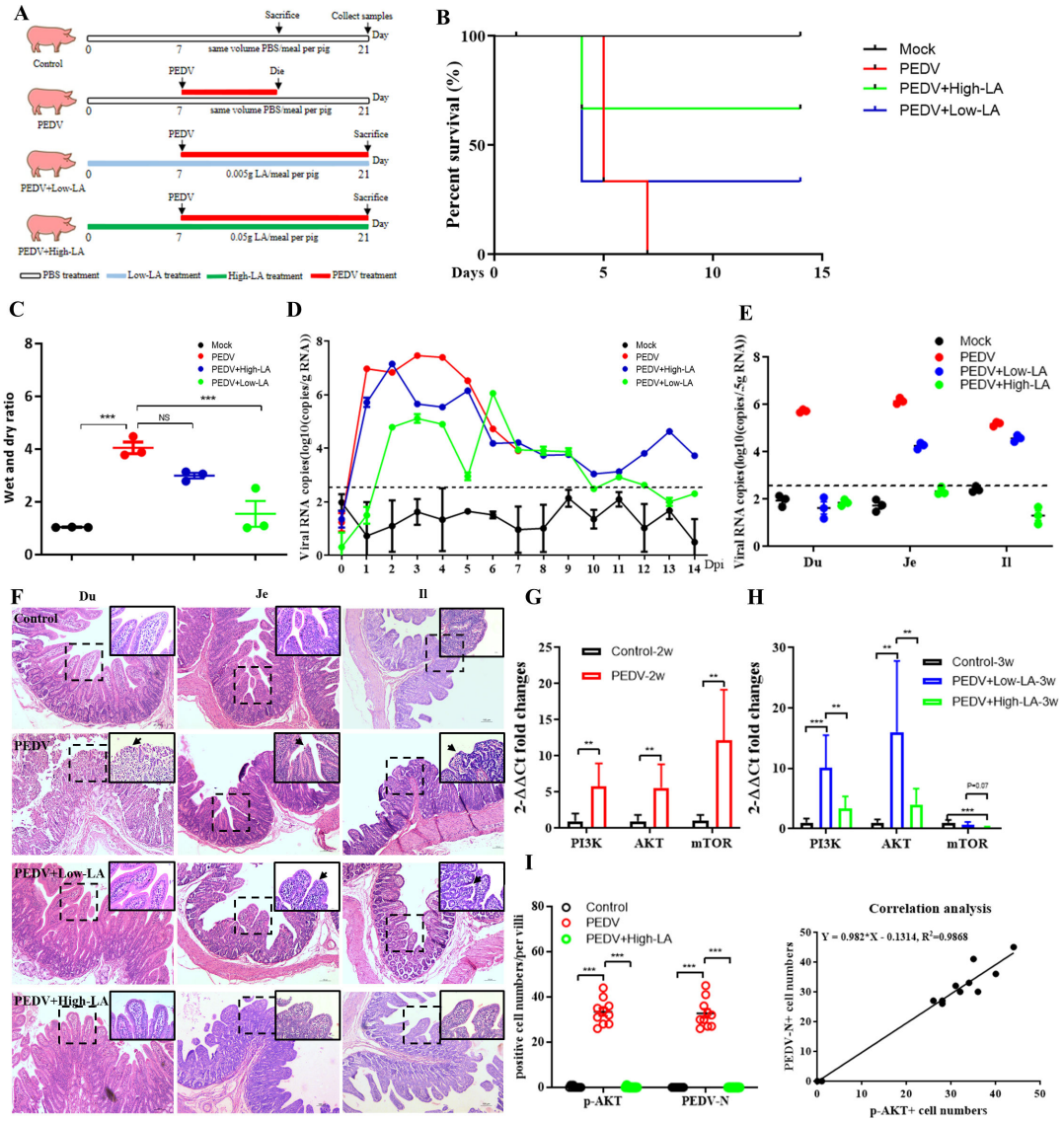

FIG 7 Linoleic acid exhibits antiviral effects against PEDV infection in animal models. (A) The flow chart of the design of the pig experiment. The survival curve (B), fecal wet and dry ratio (C), viral shedding (D), and viral load in the intestines (duodenum, jejunum, ileum) (E). The dotted lines represent the limits of detection. (F) Hematoxylin and eosin staining of different intestinal tissues is shown. Scale bars represent 100 µm. (G and H) The key molecules in different groups were detected by RT-qPCR. (I) The cells positively expressing phosphorylated AKT or viral protein in each villus were numbered and analyzed. Correlation analysis between phosphorylated AKT and viral proteins was then performed. *P* value less than 0.001 is designated with three asterisks (***). *P* value less than 0.01 is designated with two asterisks (**). *P* value less than 0.05 is designated with one asterisk (*).

Hematoxylin and eosin (H&E) staining showed that the typical characteristics of infected pigs, such as shortened intestinal villi, abscission, and deeper crypts, were not present in high-dose LA-treated pigs (Fig. 7F). Histochemistry also indicated that the virus present in the infected group was not present in the high-dose recovered pigs (Fig. S7C). Interestingly, no significant increase in IgM or PEDV-positive IgG and IgA antibodies was observed in the serum of the high-dose LA group compared to the infected group during the 2-week infection period (Fig. S7D). To explore whether other antiviral components exist in the intestines, the mRNA expression levels of the PI3K/AKT/mTOR pathway in the intestines of the different treatment groups were evaluated. Consistent with the previous *in vitro* results, the PI3K/AKT/mTOR pathway was upregulated after PEDV infection and subsequently downregulated after recovery (Fig. 7G and H). Furthermore, AKT phosphorylation was linearly correlated with PEDV infection (Fig. 7I), since phosphorylation of AKT was observed only upon PEDV infection (Fig. S7E). Taken together, LA exhibits antiviral effects against PEDV infection and restores intestinal health in pigs.

DISCUSSION

LA is an n−6 essential fatty acid, which is the major component of dietary PUFAs. It has been previously reported that polyunsaturated fatty acids docosahexaenoic acid and eicosapentaenoic acid can effectively suppress the replication of PEDV and reduce the inflammation caused by PEDV infection (15). Moreover, substances such as CH25H, which are essential for lipid synthesis, have been found to impede the invasion of PEDV (16). Our study has revealed that LA can inhibit the replication of PEDV and reduce PEDV infection *in vivo* experiments, thus helping to restore intestinal health. The proofs presented thus demonstrate the crucial role of lipid synthesis in PEDV infection.

The antiviral mechanism of LA mainly relies on the restriction of the PI3K/AKT/mTOR signaling pathway. This pathway contributes to various processes that regulate nutrient uptake, cell growth, anabolic reactions, and survival (17). Consistently, current PI3K inhibitors have the potential to control some diseases, such as cancer, human herpesvirus, porcine reproductive and respiratory syndrome virus, and severe acute respiratory syndrome coronavirus 2 (SARS-CoV-2) (18–21). AKT inhibitors have been proven to be effective in preventing viral infections, including the influenza virus and the Usutu virus (22, 23).

Moreover, LA was found to bind to and inhibit the ability of NSP5 to activate AKT. NSP5, a 3C-like protease, is involved in the cleavage of synthesized polyproteins, thereby playing an essential role in PEDV replication (24). NSP5 inhibitors are regarded as ideal broad-spectrum antiviral targets against coronavirus infection, including the coronavirus disease 2019 pandemic (25, 26). Additionally, LA was reported to bind to the S protein of SARS-CoV-2, thereby reducing its interaction with angiotensin-converting enzyme 2 *in vitro* while further restricting viral replication in synergy with remdesivir (27). LA was also demonstrated to impede HCoV-OC43 infection *in vitro*, as well as displaying positive anti-inflammatory effects *in vivo* experiments (28). This serves to reinforce the notion that LA has antiviral capabilities against coronavirus infection.

Clinical studies have shown that a higher intake or tissue levels of LA can reduce the risk of cardiovascular diseases (especially coronary artery diseases) and metabolic syndrome or type 2 diabetes (29). Additionally, LA has been found to be effective in alleviating intestinal barrier injury in early weaned squabs by down-regulating the TLR4-MyD88-JNK/p38-IL6/TNF-α pathway (30). Through two experimental cases of rats, it was determined that the topical application of sunflower seed oil, which is rich in LA, could effectively repair the damaged epidermal tissue (31). Stimulation with LA led to increased production of transforming growth factor beta 1 (TGF-β1) from dendritic cells(DCs), which in turn resulted in a greater number of Tregs being generated, showcasing their capacity to fight viruses (32). Additionally, it has been observed that the application of LA increases the formation of endoplasmic reticulum (ER)-mitochondria contacts, which in turn stimulates calcium signaling, mitochondrial energetics, and

cytotoxic T lymphocyte (CTL) effector functions (33). In addition to these functions and applications, our research has uncovered that LA can be used as a natural, edible additive to show antiviral properties (Fig. 8). The discovery of the role of linoleic acid not only enhances its existing functions but also provides a novel approach to the prevention and control of PEDV infection.

MATERIALS AND METHODS

Metabolites and reagents

Stigmasterol, succinic acid, cholic acid, palmitic acid, β-sitosterol, lactic acid, L-glutamic acid, myoinositol, linoleic acid (L1012), and elaidic acid were purchased from Merck. All substances were greater than 99% pure. Enhancers and inhibitors, including PI3K inhibitor (Merck, LY294002), AKT inhibitor (Macklin, MK-2206 2HCL), mTOR activator 3BDO (J&K Chemical, 1914077), mTOR inhibitor (Beyotime, SF2807), FH535 (J&K Chemical, 1432878), betulin (APExBIO, N1290-20), MG132, and hydroxychloroquine sulfate (CQ), were purchased from Sigma-Aldrich. 3-MA and Z-VAD-FMK were purchased from Cell Signaling Technology (CST) (14).

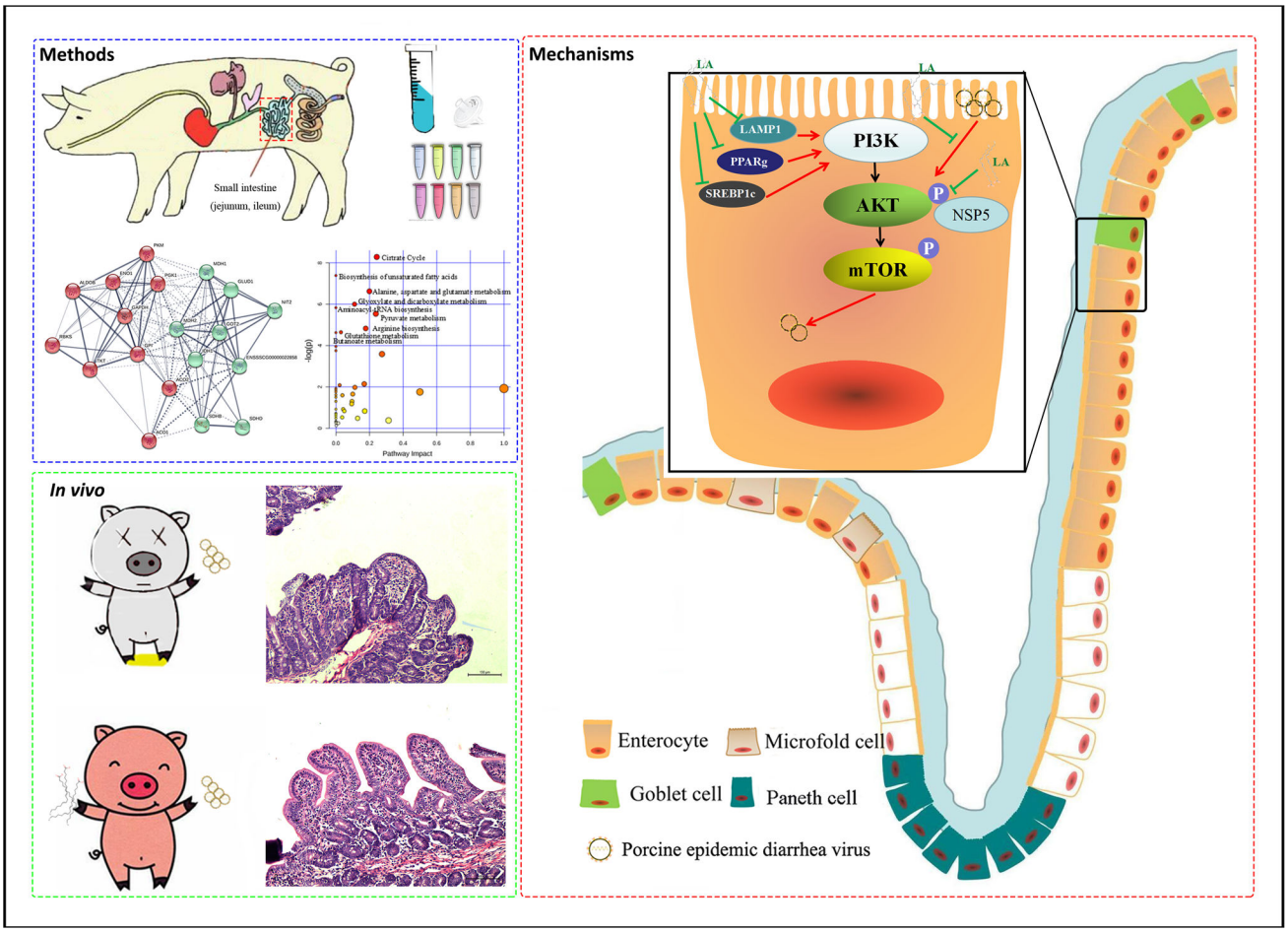

FIG 8 A schematic diagram of the mechanism by which linoleic acid inhibits PEDV infection. comparing the intestinal contents of three pig breeds, proteomic and metabolic analysis results showed that 10 metabolites involved in acid formation had the most potential to inhibit PEDV infection. Subsequently, LA was selected from these metabolites via *in vitro* experimental identification. Furthermore, we found that when PEDV infects the intestines of piglets, the presence of LA effectively inhibits viral infection. In epithelial cells (enlarged), LA inhibits viral replication and release by inhibiting activation of the PI3K pathway, especially the phosphorylation of AKT. Moreover, in clinical treatment, LA, as an oral feed compound, is able to effectively inhibit and cure PEDV infection in piglets.

Viral strains and cell culture

The cell culture-adapted PEDV strains GS-PEDV LJX and CV777 were generated and preserved in our laboratory. SeV was kindly gifted by Dr. H. Zheng from the Lanzhou Veterinary Institute, Chinese Academy of Agricultural Sciences. HSV-1 and VSV were provided by Prof. Z. Jiang from Peking University.

The African green monkey kidney cell line Vero-E6 and porcine jejunal cell line IPEC-J2 were cultured in Dulbecco's minimum essential medium (Sigma) supplemented with 10% heat-inactivated fetal bovine serum (Sigma) at 37°C under 5% CO_2. For metabolite and virus coincubation, various metabolites were mixed with the virus and incubated at room temperature for 10 min prior to infection of Vero-E6 cells.

Cell Counting Kit-8 assay

Cells incubated with intestinal content or various metabolites for the indicated time periods were detected by a CCK-8 assay (Merck, 96992) that was optimized to have a safe concentration. All procedures were performed according to the protocols from the manufacturer.

Virus titration

The viral load of a virus is generally quantified by using the $TCID_{50}$ assay. Virus samples were serially diluted 10-fold and added to cells in 96-well plates. After an incubation period, the cytopathic effect was observed, and wells with more than 50% cytopathic cells were counted and added to the calculation. The Reed–Muench method was used to analyze virus titration (34).

RNA extraction and RT-qPCR

Total RNA from cell or tissue samples was extracted using TRIzol reagent (Takara, 9109) and reverse transcribed into cDNA using random primers. The cDNAs were detected for specific genes by RT-qPCR. The detailed information was cited from reference (35). The primers are shown in Table 1.

To detect viral titers, the cDNAs were subjected to TaqMan probe-based real-time qPCR analysis for PEDV genome detection using the ABI 7500 system with TransStart Probe qPCR Supermix (TransGen Biotech). Detailed information on the primer set and probe targeting the PEDV M gene was as follows: forward primer: 5′-GAT ACT TTG GCC TCT TGT GT-3′, reverse primer: 5′-CAC AAC CGA ATG CTA TTG ACG-3′, and TaqMan probe: 5′-FAM-TTC AGC ATC CTT ATG GCT TGC ATC-TAMRA-3′. The genome copies were calculated based on a standard curve.

Coimmunoprecipitation and immunoblot analysis

Total proteins were prepared using NP-40 lysis buffer (Beyotime, P0013F) containing phenylmethylsulfonyl fluoride (PMSF; APExBIO, A2587-5.1). Protein was loaded into each lane for SDS-PAGE analysis, transferred, and immunoblotted overnight at 4°C with primary antibodies, including PI3K (Invitrogen, RL23152), p110-PI3K (4249S), AKT (9272S), phospho-AKT (12694S), mTOR (2972 s), phospho-mTOR (CST, 2971S), and GAPDH (Proteintech, 10494-1-AP). Next, the membrane was incubated with specific goat anti-mouse (Invitrogen, 31430) and goat anti-rabbit secondary antibodies (ZSGB-BIO, ZB-2301). Finally, the immunoblots were developed with chemiluminescence detection reagents (Advansta, K-12045-D50) (36).

For immunoprecipitation, cells were collected after transfection and lysed in NP-40 lysis buffer with PMSF. After centrifugation at 12,000 × *g* for 10 min, the supernatants were collected and incubated with anti-His (Proteintech 66005-1-Ig-100UL) or anti-Flag (CST, 14793S) antibodies overnight at 4°C. Subsequently, each mixture was incubated with protein A/G agarose (GenScript, L00209, L00210) for 4 h at 4°C. After incubation, the beads were washed five times and then prepared for western blotting.

Preparation of intestinal content

The intestinal contents from three breeds of 21-day-old healthy pigs (three-breed cross pigs, a specific pathogen-free pig, and *Sus scrofa*) were collected in a 15-mL centrifuge tube and centrifuged at 5,000 rpm for 20 min. Subsequently, the supernatant was aspirated, filtered through a 0.22-μm filter, and frozen at −80°C until use.

Immunofluorescence staining and confocal microscopy

Cells were covered and fixed with 4% paraformaldehyde for 15 min at room temperature (RT), rinsed with phosphate buffer saline(PBS) for 5 min, and then treated with 0.1% Triton X-100 for 15 min. Next, the samples were blocked with 5% nonfat dry milk in PBS prior to incubation with primary antibodies overnight at 4°C. The secondary antibodies were added for incubation at RT for 1 h. Subsequently, the cells were washed and stained with DAPI. After washing with PBS, the cells were visualized using an inverted fluorescence microscope or confocal laser scanning microscope (Axiovert 200, Zeiss) (37). The primary antibodies used were a mouse anti-PEDV monoclonal antibody (IgG1, k) made in our laboratory (38) and anti-His or anti-Flag monoclonal antibodies. The secondary antibodies included fluorescein isothiocyanate (FITC)-labeled goat anti-mouse IgG (H + L) antibody (Invitrogen, 4335850, 1:1,000) and phycoerythrin (PE)-labeled goat anti-rabbit antibody (Southern Biotech, 4030-09, 1:1,000 dilution).

Proteomic and metabolomic analyses

For proteomic analysis, the filtered intestinal contents were subjected to protein extraction, protein quantification, and trypsin digestion to obtain the samples. Each sample was separated with an HPLC system using a nanoliter flow rate. The sample was loaded by the autosampler into the mass spectrometer precolumn and separated by the analytical column. Each sample was separated by capillary high-performance liquid chromatography and subjected to mass spectrometry analysis using an Orbitrap Fusion Lumos mass spectrometer (Thermo Scientific).

For metabolomic analysis, a 100-μL sample was mixed with 350 μL of precooled methanol and 10 μL of L-2-chlorophenylalanine (1 mg/mL stock), vortexed for 30 s, ultrasonicated for 10 min in ice water, and centrifuged at 4°C for 15 min at 10,000 rpm. Subsequently, 300 μL of the supernatant was placed in a fresh tube. After evaporation, 40 μL of methoxyamination hydrochloride (20 mg/mL in pyridine) was added, and the sample was incubated at 80°C for 30 min and then derivatized with 60 μL of bis-(trimethylsilyl)-trifluoroacetamide (BSTFA) reagent (1% trimethylchlorosilane [TMCS], vol/vol) at 70°C for 1.5 h. All samples were analyzed by gas chromatography coupled with time-of-flight mass spectrometry using an Agilent 7890 gas chromatograph and a time-of-flight mass spectrometer (39). Raw data analysis, including peak extraction, baseline adjustment, deconvolution, alignment, and integration, was completed with Chroma TOF software (V 4.3 x, LECO), and the LECO-Fiehn Rtx5 database was used for metabolite identification by matching the mass spectrum and retention time (40).

TABLE 1 Primers of RT-qPCR for the mRNA expression detection of molecules

Name	Forward primer	Reverse primer
LAMP1	CGTGTCACGAAGGCGTTTTCAG	CTGTTCTCGTCCAGCAGACACT
PPARγ	ACACTGTGTATGGCTGAGAAGA	GACGGTCTCCACTGACGTG
SREBP1c	GGAGCCATGGATTGCACTTT	ATGTGGCAGGAGGTGGAGAC
FABP4	TACTGAGATTTCCTTCATACTGGGC	GCTCTCTCATAAACTCTCGTGGAAG
PI3K	TCCGGAACTGTGTAATGAACAGGA	ATGGCAGCCTCTATGGCAATC
AKT	ACTGTCATCGAACGCACCTT	CTCCTCCTCCTCCTGCTTCT
mTOR	CTGGGACTCAAATGTGTGCAGTTC	GAACAATAGGGTGAATGATCC GGG
GAPDH	CATCCATGACAACTTCGGCA	GCATGGACTGTGGTCATGAGTC

In silico docking and ITC assay

The Protein Data Bank contains a very large library of protein structures. Because the protein crystal structure of the PEDV-LJX we used was not available, SWISS MODEL was used to simulate the crystal structures of PEDV structural and nonstructural proteins, including S1, S2, M, N, E, NSP1-16, and ORF3 (41). The three-dimensional structure of LA was obtained from PubChem. AutoDock Vina and Discovery Studio were used to dock LA into the active pocket of the potential viral proteins. The potential LA-protein docking results were visualized by PyMOL 2 (42). For the ITC experiment, eukaryotic NSP5 was obtained by establishing an overexpressing human embryonic kidney 293 cell line (HEK293 cell line). Following the preparation of LA and total cell protein, we proceed to detect their interaction using the molecular interaction isothermal titration instrument in accordance with the instrument's usage guidelines. After comparison to the protein from the empty HEK293 cell line, the ITC result was analyzed and displayed by NanoAnalyze software.

Inactivation of virus

The virus was inactivated under UV at a wavelength of 254 nm for 30 min. The inactivated virus was identified by western blotting and $TCID_{50}$ (43).

Enzyme-linked immunosorbent assay

The antibody levels of PEDV-IgA (MLBio, ML863241), PEDV-IgG (MLBio, ML930546), and PEDV-IgM (Bethyl, E101-117) were measured by enzyme-linked immunosorbent assay kits according to the manufacturer's instructions (44).

Histological analysis and immunohistochemistry

Different segments of intestinal tissue were collected, fixed for 24 h in 10% formalin, dehydrated according to the standard protocol, and then embedded in paraffin. The sections were cut from each tissue block, deparaffinized in xylene, stained with H&E, and analyzed under a microscope to evaluate pathological changes. In addition, the sections were renatured to expose pathogens and stained with anti-PEDV-N primary antibody (1:200) to observe viral infection conditions in the intestines. The stained sections were analyzed under an optical microscope (45).

Animal experimental details

Common enteric viruses, including PEDV-free newborn piglets (Duroc-Landrace-Yorkshire), screened by real-time RT-qPCR, were purchased from a pig farm located in Dingxi, Gansu Province, housed in isolated animal rooms, and fed with milk substitute from Bolai Yaoye. The gender of the pigs was chosen randomly.

Fifteen newborn piglets were divided into four groups: the control group (n = 6), the infected group (n = 3), the low-dose linoleic acid antiviral group (n = 3) (0.005 g/dose, three times a day), and the high-dose linoleic acid antiviral group (n = 3) (0.05 g/dose, three times a day). LA at different doses was orally administered throughout the 21-day period, while an equal volume of PBS was used in the control group. Pigs were challenged with 10^9 copies/mL of the GS PEDV LJX strain via oral administration on day 7. The body temperature and clinical symptoms were recorded every 8 h after the challenge, and anal swabs were collected to detect viral shedding. The clinical symptoms included fecal scores, which were independently and blindly characterized as follows: 0, normal feces; 1, mixed stool sample containing both solid and pasty feces; 2, semiliquid feces; and 3, liquid feces. In addition, wet/dry ratios were used to determine the occurrence of diarrhea (35). On day 14, all the infected piglets were dying and were therefore sacrificed. All intestines and intestinal contents from the control groups (3/6) and infected groups were collected for later analysis.

TABLE 2 Abbreviations

Abbreviation	Definition	Abbreviation	Definition
PED	Porcine epidemic diarrhea	Co-IP	Coimmunoprecipitation
PEDV	Porcine epidemic diarrhea virus	ITC	Isothermal titration calorimetry
IPEC-J2	Porcine intestinal epithelial cells	NSP	Nonstructural protein
HSV	Herpes simplex virus	VSV	Vesicular stomatitis virus
SeV	Sendai virus	TC	Three-breed cross pig
SPF	Specific-pathogen-free pig	SS	*Sus scrofa*
PPARγ	Peroxisome proliferator activated receptor gamma	FABP4	Fatty acid binding protein 4
LAMP1	Lysosomal-associated membrane protein 1	FFAR1	Free fatty acid receptor
PUFAs	Polyunsaturated fatty acids	SREBP1c	Sterol regulatory element binding protein 1 c
EPA	Eicosapentaenoic acid	CQ	Chloroquine
DHA	Docosahexaenoic acid	CCK-8	Cell Counting Kit-8
ACE2	Angiotensin-converting enzyme 2	DMEM	Dulbecco's minimum essential medium
FBS	Fetal bovine serum	$TCID_{50}$	Median tissue culture infectious dose

The remaining 3/6 control pigs were sacrificed at 21 days. The recovered pigs were kept for 14 days after the infection and then sacrificed. To obtain a more detailed understanding of the physiological changes in pigs that had recovered from viral infection, intestinal segments and serum samples of uninfected pigs and recovered pigs were collected for comparison. All experimental procedures and animal care protocols were approved by the guidelines for Care and Use of Laboratory Animals of Lanzhou Veterinary Research Institute, Chinese Academy of Agricultural Sciences, China.

Quantification and statistical analysis

Venn diagrams were used to show the logical relationships between different groups of metabolites and proteins according to standard procedures (https://bioinfogp.cnb.csic.es/tools/venny/index.html). To analyze the relationships between these metabolites and their enriched pathways, MetaboAnalyst was used (https://www.metaboanalyst.ca/). Furthermore, Kyoto Encyclopedia of Genes and Genomes and GO analyses were performed on these related proteins (https://string-db.org/). All data and diagrams were analyzed and shown with GraphPad 7.0 and SPSS. Analysis of significant differences was performed by one-way analysis of variance (***, $P < 0.001$; **, $P < 0.01$; *, $P < 0.05$, $n \geq 3$). The data are presented as the mean ± SEM. All abbreviations were summarized in Table 2.

ACKNOWLEDGMENTS

This work was supported by the National Natural Science Foundation of China (U22A20522, 31972689), the Joint Science Foundation of Gansu Province (23JRRA1516), the Science and Technology Major Project of Gansu Province (22ZD6NA001), and the WUR-CAAS joint Ph.D. Program and the China Scholarship Council. We thank the experimental platform from Lanzhou Veterinary Research Institute, Chinese Academy of Agricultural Sciences.

We thank colleagues for helping in the animal experiment from the Animal Immunology Group, including Baoyu Li, Yuguang Fu, Jianing Chen, Yabin Lu, Maolin Li, Tao Zhang, Jing Zhao, Yaru Cui, Zemei Wang, Huazheng Jiang, Haoyuan Yu, Manita Aryal, and Chao Gong. We thank colleagues for providing comments on the manuscript, including Ning Yang, Yunhang Zhang, Chen Tan, and Yifei Cai.

S.Y. and G.L. conceived this paper. S.Y. designed and conducted the experiments, analyzed the data, and drafted the manuscript. S.Y., C.W., and X.H. isolated the primary cells. S.L. assisted with paraffin section staining. C.J. and H.S. contributed to discussions and revised the manuscript.

AUTHOR AFFILIATIONS

[1]State Key Laboratory of Animal Disease Control and Prevention, College of Veterinary Medicine, Lanzhou University, Lanzhou Veterinary Research Institute, Chinese Academy of Agricultural Science, Lanzhou, China
[2]Cell Biology and Immunology Group, Wageningen University and Research, Wageningen, the Netherlands
[3]Key Laboratory of Veterinary Biological Engineering and Technology, Ministry of Agriculture, Institute of Veterinary Medicine, Jiangsu Academy of Agricultural Sciences, Nanjing, Jiangsu, China
[4]College of Veterinary Medicine, Xinjiang Agricultural University, Urumqi, China

AUTHOR ORCIDs

Shanshan Yang http://orcid.org/0009-0000-7748-0223
Guangliang Liu http://orcid.org/0000-0001-8158-5749

FUNDING

Funder	Grant(s)	Author(s)
MOST | National Natural Science Foundation of China (NSFC)	U22A20522, 31972689	Guangliang Liu
Joint Science Foundation of Gansu Province	23JRRA1516	Guangliang Liu
Science and Technology Major Project of Gansu Province	22ZD6NA001	Guangliang Liu

ADDITIONAL FILES

The following material is available online.

Supplemental Material

Supplemental figures (JVI01700-23-S0001.pdf). Figures S1 to S7.

REFERENCES

1. Li Z, Ma Z, Li Y, Gao S, Xiao S. 2020. Porcine epidemic diarrhea virus: molecular mechanisms of attenuation and vaccines. Microb Pathog 149:104553. https://doi.org/10.1016/j.micpath.2020.104553
2. Jung K, Saif LJ. 2015. Porcine epidemic diarrhea virus infection: etiology, epidemiology, pathogenesis and immunoprophylaxis. Vet J 204:134–143. https://doi.org/10.1016/j.tvjl.2015.02.017
3. Wang P, Bai J, Liu X, Wang M, Wang X, Jiang P. 2020. Tomatidine inhibits porcine epidemic diarrhea virus replication by targeting 3CL protease. Vet Res 51:136. https://doi.org/10.1186/s13567-020-00865-y
4. Choi H-J, Kim J-H, Lee C-H, Ahn Y-J, Song J-H, Baek S-H, Kwon D-H. 2009. Antiviral activity of quercetin 7-rhamnoside against porcine epidemic diarrhea virus. Antiviral Res 81:77–81. https://doi.org/10.1016/j.antiviral.2008.10.002
5. Li L, Yu X, Zhang H, Cheng H, Hou L, Zheng Q, Hou J. 2019. *In vitro* antiviral activity of griffithsin against porcine epidemic diarrhea virus. Virus Genes 55:174–181. https://doi.org/10.1007/s11262-019-01633-7
6. Kwon H-J, Ryu YB, Kim Y-M, Song N, Kim CY, Rho M-C, Jeong J-H, Cho K-O, Lee WS, Park S-J. 2013. *In vitro* antiviral activity of phlorotannins isolated from *Ecklonia cava* against porcine epidemic diarrhea coronavirus infection and hemagglutination. Bioorg Med Chem 21:4706–4713. https://doi.org/10.1016/j.bmc.2013.04.085
7. Possemiers S, Grootaert C, Vermeiren J, Gross G, Marzorati M, Verstraete W, Van de Wiele T. 2009. The intestinal environment in health and disease - recent insights on the potential of intestinal bacteria to influence human health. Curr Pharm Des 15:2051–2065. https://doi.org/10.2174/138161209788489159
8. Thursby E, Juge N. 2017. Introduction to the human gut microbiota. Biochem J 474:1823–1836. https://doi.org/10.1042/BCJ20160510
9. Rastelli M, Cani PD, Knauf C. 2019. The gut microbiome influences host endocrine functions. Endocr Rev 40:1271–1284. https://doi.org/10.1210/er.2018-00280
10. Li N, Ma W-T, Pang M, Fan Q-L, Hua J-L. 2019. The commensal microbiota and viral infection: a comprehensive review. Front Immunol 10:1551. https://doi.org/10.3389/fimmu.2019.01551
11. Yuan L, Zhang S, Wang Y, Li Y, Wang X, Yang Q. 2018. Surfactin inhibits membrane fusion during invasion of epithelial cells by enveloped viruses. J Virol 92:e00809-18. https://doi.org/10.1128/JVI.00809-18
12. Xu F, Na L, Li Y, Chen L. 2020. Roles of the PI3K/AKT/mTOR signalling pathways in neurodegenerative diseases and tumours. Cell Biosci 10:54. https://doi.org/10.1186/s13578-020-00416-0
13. Daina A, Michielin O, Zoete V. 2019. SwissTargetPrediction: updated data and new features for efficient prediction of protein targets of small molecules. Nucleic Acids Res 47:W357–W364. https://doi.org/10.1093/nar/gkz382
14. Zhang N, Shi H, Yan M, Liu G. 2021. IFIT5 negatively regulates the type I IFN pathway by disrupting TBK1-IKKε-IRF3 signalosome and degrading IRF3 and IKKε. J Immunol 206:2184–2197. https://doi.org/10.4049/jimmunol.2001033
15. Suo X, Wang J, Wang D, Fan G, Zhu M, Fan B, Yang X, Li B. 2023. DHA and EPA inhibit porcine coronavirus replication by alleviating ER stress. J Virol:e0120923. https://doi.org/10.1128/jvi.01209-23
16. Zhang Y, Song Z, Wang M, Lan M, Zhang K, Jiang P, Li Y, Bai J, Wang X. 2019. Cholesterol 25-hydroxylase negatively regulates porcine intestinal coronavirus replication by the production of 25-hydroxycholesterol. Vet Microbiol 231:129–138. https://doi.org/10.1016/j.vetmic.2019.03.004

17. Yu JSL, Cui W. 2016. Proliferation, survival and metabolism: the role of PI3K/AKT/mTOR signalling in pluripotency and cell fate determination. Development 143:3050–3060. https://doi.org/10.1242/dev.137075
18. Zhu L, Yang S, Tong W, Zhu J, Yu H, Zhou Y, Morrison RB, Tong G. 2013. Control of the PI3K/AKT pathway by porcine reproductive and respiratory syndrome virus. Arch Virol 158:1227–1234. https://doi.org/10.1007/s00705-013-1620-z
19. Vanhaesebroeck B, Perry MWD, Brown JR, André F, Okkenhaug K. 2021. PI3K inhibitors are finally coming of age. Nat Rev Drug Discov 20:741–769. https://doi.org/10.1038/s41573-021-00209-1
20. Mabuchi S, Kuroda H, Takahashi R, Sasano T. 2015. The PI3K/AKT/mTOR pathway as a therapeutic target in ovarian cancer. Gynecol Oncol 137:173–179. https://doi.org/10.1016/j.ygyno.2015.02.003
21. Fattahi S, Khalifehzadeh-Esfahani Z, Mohammad-Rezaei M, Mafi S, Jafarinia M. 2022. PI3K/AKT/mTOR pathway: a potential target for anti-SARS-CoV-2 therapy. Immunol Res 70:269–275. https://doi.org/10.1007/s12026-022-09268-x
22. Hirata N, Suizu F, Matsuda-Lennikov M, Edamura T, Bala J, Noguchi M. 2014. Inhibition of AKT kinase activity suppresses entry and replication of influenza virus. Biochem Biophys Res Commun 450:891–898. https://doi.org/10.1016/j.bbrc.2014.06.077
23. Albentosa-González L, Sabariegos R, Arias A, Clemente-Casares P, Mas A. 2021. Akt interacts with usutu virus polymerase, and its activity modulates viral replication. Pathogens 10:244. https://doi.org/10.3390/pathogens10020244
24. Wang D, Fang L, Shi Y, Zhang H, Gao L, Peng G, Chen H, Li K, Xiao S. 2016. Porcine epidemic diarrhea virus 3C-like protease regulates its interferon antagonism by cleaving NEMO. J Virol 90:2090–2101. https://doi.org/10.1128/JVI.02514-15
25. Anand K, Ziebuhr J, Wadhwani P, Mesters JR, Hilgenfeld R. 2003. Coronavirus main proteinase (3CLpro) structure: basis for design of anti-SARS drugs. Science 300:1763–1767. https://doi.org/10.1126/science.1085658
26. Yan F, Gao F. 2021. An overview of potential inhibitors targeting non-structural proteins 3 (PL(pro) and Mac1) and 5 (3Cl(pro)/M(pro)) of SARS-CoV-2. Computational and Structural Biotechnology Journal 19:4868–4883. https://doi.org/10.1016/j.csbj.2021.08.036
27. Toelzer C, Gupta K, Yadav SKN, Borucu U, Davidson AD, Kavanagh Williamson M, Shoemark DK, Garzoni F, Staufer O, Milligan R, Capin J, Mulholland AJ, Spatz J, Fitzgerald D, Berger I, Schaffitzel C. 2020. Free fatty acid binding pocket in the locked structure of SARS-CoV-2 spike protein. Science 370:725–730. https://doi.org/10.1126/science.abd3255
28. Goc A, Sumera W, Rath M, Niedzwiecki A. 2022. Linoleic acid binds to SARS-CoV-2 RdRp and represses replication of seasonal human coronavirus OC43. Sci Rep 12:19114. https://doi.org/10.1038/s41598-022-23880-9
29. Marangoni F, Agostoni C, Borghi C, Catapano AL, Cena H, Ghiselli A, La Vecchia C, Lercker G, Manzato E, Pirillo A, Riccardi G, Risé P, Visioli F, Poli A. 2020. Dietary linoleic acid and human health: focus on cardiovascular and cardiometabolic effects. Atherosclerosis 292:90–98. https://doi.org/10.1016/j.atherosclerosis.2019.11.018
30. Xu Q, Zhao J, Jian H, Ye J, Gong M, Zou X, Dong X. 2023. Linoleic acid ameliorates intestinal mucosal barrier injury in early weaned pigeon squabs (*Columba livia*). J Anim Sci 101:skad125. https://doi.org/10.1093/jas/skad125
31. Prottey C, Hartop PJ, Black JG, McCormack JI. 1976. The repair of impaired epidermal barrier function in rats by the cutaneous application of linoleic acid. Br J Dermatol 94:13–21. https://doi.org/10.1111/j.1365-2133.1976.tb04336.x
32. Yang S, Wang C, Huang X, Jansen CA, Savelkoul HFJ, Liu G. 2023. Linoleic acid stimulation results in TGF-B1 production and inhibition of PEDV infection *in vitro*. Virology 581:89–96. https://doi.org/10.1016/j.virol.2023.03.004
33. Nava Lauson CB, Tiberti S, Corsetto PA, Conte F, Tyagi P, Machwirth M, Ebert S, Loffreda A, Scheller L, Sheta D, et al. 2023. Linoleic acid potentiates $CD8^+$ T cell metabolic fitness and antitumor immunity. Cell Metab 35:633–650. https://doi.org/10.1016/j.cmet.2023.02.013
34. Lei C, Yang J, Hu J, Sun X. 2021. On the calculation of TCID50 for quantitation of virus infectivity. Virol. Sin 36:141–144. https://doi.org/10.1007/s12250-020-00230-5
35. Yang S, Li Y, Wang B, Yang N, Huang X, Chen Q, Geng S, Zhou Y, Shi H, Wang L, Brugman S, Savelkoul H, Liu G. 2020. Acute porcine epidemic diarrhea virus infection reshapes the intestinal microbiota. Virology 548:200–212. https://doi.org/10.1016/j.virol.2020.07.001
36. Li Y, Yang S, Huang X, Yang N, Wang C, Zhao J, Jing Z, Willems L, Liu G. 2021. MyD88 mediates colitis- and RANKL-induced microfold cell differentiation. Vet Sci 9:6. https://doi.org/10.3390/vetsci9010006
37. Copple SS, Sawitzke AD, Wilson AM, Tebo AE, Hill HR. 2011. Enzyme-linked immunosorbent assay screening then indirect immunofluorescence confirmation of antinuclear antibodies: a statistical analysis. Am J Clin Pathol 135:678–684. https://doi.org/10.1309/AJCP6R8EELGODAYW
38. Yang W, Chen W, Huang J, Jin L, Zhou Y, Chen J, Zhang N, Wu D, Sun E, Liu G. 2019. Generation, identification, and functional analysis of monoclonal antibodies against porcine epidemic diarrhea virus nucleocapsid. Appl Microbiol Biotechnol 103:3705–3714. https://doi.org/10.1007/s00253-019-09702-5
39. Kind T, Wohlgemuth G, Lee DY, Lu Y, Palazoglu M, Shahbaz S, Fiehn O. 2009. Fiehnlib: mass spectral and retention index libraries for metabolomics based on quadrupole and time-of-flight gas chromatography/mass spectrometry. Anal Chem 81:10038–10048. https://doi.org/10.1021/ac9019522
40. Beckonert O, Keun HC, Ebbels TMD, Bundy J, Holmes E, Lindon JC, Nicholson JK. 2007. Metabolic profiling, metabolomic and metabonomic procedures for NMR spectroscopy of urine, plasma, serum and tissue extracts. Nat Protoc 2:2692–2703. https://doi.org/10.1038/nprot.2007.376
41. Waterhouse A, Bertoni M, Bienert S, Studer G, Tauriello G, Gumienny R, Heer FT, de Beer TAP, Rempfer C, Bordoli L, Lepore R, Schwede T. 2018. SWISS-MODEL: homology modelling of protein structures and complexes. Nucleic Acids Res 46:W296–W303. https://doi.org/10.1093/nar/gky427
42. Buzko OV, Bishop AC, Shokat KM. 2002. Modified autodock for accurate docking of protein kinase inhibitors. J Comput Aided Mol Des 16:113–127. https://doi.org/10.1023/a:1016366013656
43. Tseng CC, Li CS. 2007. Inactivation of viruses on surfaces by ultraviolet germicidal irradiation. J Occup Environ Hyg 4:400–405. https://doi.org/10.1080/15459620701329012
44. Alhajj M, Farhana A. 2021. Enzyme linked immunosorbent assay. In . StatPearls, Treasure Island (FL).
45. Lupariello F, Godio L, Di Vella G. 2021. Immunohistochemistry patterns of SARS-CoV-2 deaths in forensic autopsies. Leg Med (Tokyo) 51:101894. https://doi.org/10.1016/j.legalmed.2021.101894